Antiproton-nucleus elastic and inelastic scattering at intermediate energies

Zhang Yu-shun,[1,2] Liu Ji-feng,[3] B. A. Robson,[3] and Li Yang-guo[2]
[1]*CCAST (World Laboratory) Center of Theoretical Physics, P.O. Box 8730, 100 080 Beijing, China*
[2]*Institute of High Energy Physics, Academia Sinica, P.O. Box 918(4-1), 100 039 Beijing, China*
[3]*Department of Theoretical Physics, Research School of Physical Sciences and Engineering, The Australian National University, Canberra, Australian Capital Territory 0200, Australia*
(Received 27 November 1995)

Using the experimental $\bar{p}N$ amplitude and multiple scattering theory, we obtained the antiproton optical potential at incident energies from 180 to 1800 MeV with the impulse approximation. It is found that the imaginary parts of the optical potential strengths are nearly constant between 130 and 140 MeV. The elastic data of the 180 MeV antiproton on ^{12}C, ^{16}O, ^{40}Ca, and ^{208}Pb and the inelastic data of the 180 MeV antiproton on ^{12}C are analyzed within the framework of the eikonal approximation. The collective excitations to one-phonon levels are treated using the antiproton optical potential with the adiabatic approximation. The differential cross section of elastic scattering of 180 to 1833 MeV antiproton on ^{12}C, on ^{16}O, ^{40}Ca, and ^{208}Pb and the inelastic scattering of 180 to 1833 MeV antiproton ^{12}C are predicted.

PACS number(s): 13.75.Cs, 25.43.+t, 24.10.Ht

I. INTRODUCTION

With the operation of the CERN Low-Energy Antiproton Storage Ring LEAR, differential cross sections were measured for the elastic and inelastic scattering of antiprotons at energies of $T_{\bar{p}}=179.7$ MeV on the nuclei ^{12}C, ^{20}Ca, and ^{208}Pb. From the data [1–5] it can be seen that the differential cross sections reveal a pronounced diffractive behavior (in contrast with proton-nucleus scattering at the same energies). These data already provide evidence for the strong-absorptive aspect of the $\bar{p}$-nucleus interaction. In Ref. [6] it was found that the potentials are well determined at the nuclear surface around the strong-absorption radius, where the imaginary part of the potential $W(R)$ is at least twice as large as the real part $V(R)$. It is obvious that all data favor the D-type potential (strong imaginary and weak real strengths) over the S-type potential (strong real and weak imaginary strengths) [7].

The study of medium-energy antiproton-nucleus interactions in terms of the optical potential is a topic of current interest [8]. The aim of the present work is to obtain antiproton optical potentials at incident energies from 180 to 1800 MeV with the impulse approximation, by using $\bar{p}N$ two-body elementary amplitudes from microscopic consideration. By using these optical potentials, the elastic data of the 180 MeV antiproton on ^{12}C, ^{16}O, ^{40}Ca, and ^{208}Pb and the inelastic data of the 180 MeV antiproton on ^{12}C are analyzed within the framework of the eikonal approximation. The nuclear excitation is described in terms of the collective model with the adiabatic approximation. Further, the differential cross sections of elastic scattering of 180–1833 MeV antiprotons on ^{12}C, ^{16}O, ^{40}Ca, and ^{208}Pb and inelastic scattering of 180–1833 MeV antiprotons on ^{12}C are predicted.

The paper is organized as follows. In Sec. II the optical potential of the $\bar{p}$-nucleus interaction corresponding to the impulse approximation is derived. In Sec. III we discuss the elastic and inelastic processes in the framework of the eikonal approximation with the collective model. The last section contains a conclusion of the results.

II. THE OPTICAL POTENTIAL OF THE $\bar{p}$-NUCLEUS INTERACTION

The optical potential of the $\bar{p}$-nucleus interaction with multiple scattering theory can be written in the form [9]

$$U_{\bar{p}}^{\rm opt}=\langle\psi_0|\sum_{i=1}^{A} t_{\bar{p}N}(i)|\psi_0\rangle, \tag{2.1}$$

where ψ_0 is the wave function of the ground state, $t_{\bar{p}N}$ the t matrix of the antiproton-nucleon interaction, corresponding to the $\bar{p}N$ scattering amplitude determined by antiproton-nucleon scattering experiments, and the $\bar{p}N$ elementary amplitude is of the form

$$f_{\bar{p}N}=\frac{ik\sigma_{\bar{p}N}}{4\pi}(1-i\epsilon)e^{-\beta^2q^2/2}. \tag{2.2}$$

The values for $\sigma_{\bar{p}N}$, the total $\bar{p}N$ cross section, ϵ, the ratio of the real-imaginary $\bar{p}N$ forward amplitude, and β, the value of the diffraction-slope parameter, and experimental parameters [10,11] are listed in Table I. Using the relation between Eq. (2.1) and the t matrix, with the impulse approximation, the optical potential of the $\bar{p}$-nucleus interaction can be written as follows [12]:

TABLE I. The data of $\bar{p}N$ amplitude [13–15].

Kinetic T(MeV)	Momentum (MeV/c)	$\sigma_{\bar{p}N}$ (mb)	ϵ	β^2 (GeV/c)$^{-2}$	W_0 (MeV)
179.7	607.8	149	0.2	22.2	129.6
294.8	800	132	0.25	16.2	137.3
508	1100.5	110	0.22	15.2	133
1070	1775	92	0.14	13.2	131
1833	2607	81	0.04	13.1	122

$$U_{\bar{p}}^{\rm opt}(r)=\frac{2\pi\hbar}{m}f_{\bar{p}N}(0)\rho(r)=i\hbar v_{\bar{p}}\frac{\sigma_{\bar{p}N}(1-i\epsilon)}{2}\rho(r)$$
$$=V(r)+iW(r), \qquad (2.3)$$

where $v_{\bar{p}}$ is the velocity of the antiproton and $\rho(r)$ the nuclear density. [$\rho(r)$ is normalized to the number of nucleons in the nucleus.] The nucleus density is given by the Woods-Saxon formula

$$\rho(r)=\rho_0 f_j \quad (j=v \text{ or } w), \qquad (2.4)$$

with radial form factors of the Woods-Saxon type, i.e.,

$$f_j=\left\{1+\exp\left[\frac{r-R_j}{a_j}\right]\right\}^{-1} \qquad (2.5)$$

$\rho_0\simeq 0.16$ fm^{-3} and $R_j=r_jA^{1/3}$, where A is the number of nucleons, r_j is the radius, and a_j is the diffuseness parameter. Then the optical potential of the antiproton-nucleus interaction can be expressed as

$$U_{\bar{p}}^{\rm opt}(r)=-V_0 f_v(r)-iW_0 f_w(r), \qquad (2.6)$$

where

$$V_0=\hbar v_{\bar{p}}\frac{\sigma_{\bar{p}N}}{2}\rho_0,\epsilon \qquad (2.7)$$

$$W_0=\hbar v_{\bar{p}}\frac{\sigma_{\bar{p}N}}{2}\rho_0. \qquad (2.8)$$

The optical potential depths V_0 and W_0 are determined definitely by the $\bar{p}N$ elementary amplitude.

From the $\bar{p}$-N experimental data listed in Table I, it can be seen that $\sigma_{\bar{p}N}$ has played an important role in the depths V_0 and W_0, and we can get the optical potential strengths. Accordingly Eq. (2.8) allows us to calculate the imaginary part of the potential, listed in the last column of Table I. The results show the imaginary part W_0 in the interval from 180 to 1833 MeV fluctuating around 130 MeV. Therefore, W_0 in our calculation can be considered a constant theoretically, taken as 135 MeV. From Table I it can be seen also that the ratio of $|V_0|/|W_0|$ is equal to ϵ. Therefore W_0 is at least fourfold times larger than V_0. As a result, such an antiproton optical potential is strongly absorptive. Using Eqs. (2.7) and (2.8), the calculated real V_0 and imaginary W_0 potentials at 180 MeV are given in Fig. 1, as solid curves. The dot-dashed curves show the theoretical potential corresponding to the Glauber amplitude [Re$V_N(r)=0$ since $\epsilon=0$] calculated in Ref. [6]. The dashed curves show the phenomenological potential from Ref. [2]. In Fig. 1, it can be seen that the results we get are the same as the calculation carried out above in the Glauber approximation in Ref. [6].

At the same time, the magnitude and sign of V_0 and W_0 are determined by the behavior of ϵ and $\sigma_{\bar{p}N}$ for the $\bar{p}N$ elementary amplitude, and these two parameters have been determined by the experimental data [10,11]. Therefore the real V_0 and imaginary W_0 of the potential in our calculation are not only the most convenient to calculate but also without any adjustable free parameter.

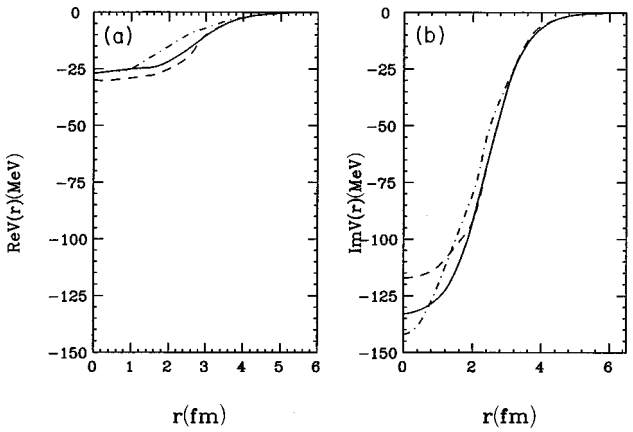

FIG. 1. Optical potential for $\bar{p}^{12}$C scattering at $T_{\bar{p}}=179.7$ MeV. The solid curves are our results; the dot-dashed curves show the theoretical potential corresponding to the Glauber amplitude [Re$V_N(r)=0$ since $\epsilon=0$] calculated in Ref. [6]. The dashed curves show the phenomenological potential from Ref. [2].

III. ELASTIC AND INELASTIC SCATTERING

In the present work, we shall assume that the antiproton-nucleus interaction is described by an optical potential $U_{\bar{p}}^{\rm opt}$ which is, in general, nonspherical. We assume that the deformed optical potential $U_{\bar{p}}^{\rm opt}$ can be expanded as

$$U_{\bar{p}}^{\rm opt}(r)\simeq U_0(r)-\sum_{\lambda\mu}\beta_\lambda U_{\lambda\mu}, \qquad (3.1)$$

where

$$U_{\lambda\mu}=R_0\frac{d}{dr}U_0(r)D^{\lambda}_{\mu 0}(\theta_i)Y_{\lambda\mu}(\theta,\varphi). \qquad (3.2)$$

Here $D^{\lambda}_{\mu 0}(\theta_i)$ is a rotation matrix and θ_i stands for the Euler angles between the body-fixed and space-fixed coordinates.

For rotational nuclei there exist a large number of low-lying levels easily excited by a medium-energy projectile. These states must be summed over in both the intermediate and final states. To accomplish this we use the closure approximation, which implies that the orientation of the nucleus is not changed during the scattering process. For an axially symmetric nucleus with quadrupole deformation $\lambda=2$, a further hypothesis $z\simeq 0$ is made; then the operator for the scattering amplitude between the nucleus and antiproton may be written as [16] (in the eikonal approximation)

$$\hat{F}(q,\Phi')=\frac{ik}{2\pi}\int d^2b e^{i\vec{q}\cdot\vec{b}}\{1-\exp[-\chi_0(b)-\chi_1(b)t(\Phi')]\} \qquad (3.3)$$

where

$$\chi_0(b)=\frac{i}{2k}\int_{-\infty}^{\infty}dz U_0(r), \qquad (3.4)$$

$$\chi_1(b)=\frac{i\beta_2 R_0}{2k}\int_{-\infty}^{\infty}dz\frac{d}{dr}U_0(r)\frac{1}{4}\left(\frac{5}{4\pi}\right)^{1/2}, \qquad (3.5)$$

$$t(\Phi')=1+\frac{3}{\pi}\cos(2\Phi'), \tag{3.6}$$

where $t(\Phi')$ will depend only on $\Phi-\varphi$, the difference between the nuclear azimuthal coordinate and the projectile, by virtue of our choice of z axis.

In an exclusive scattering we must project the $\hat{F}$ operator of Eq. (3.3) onto nuclear states of definite LM. Since the target states are in the ground state $(L,M=0,0)$, we can only go to the excited state (L even). In this case, we can also write $Y_{LM}(\theta_i)=P_{LM}(\theta)e^{im\varphi}$. If we change the variable to $\Phi'=\Phi-\varphi$ and $\theta'_i(\theta,\Phi')$, the scattering amplitude may be expressed formally as

$$F_{LM}(q)=ik(i)^M\int d\theta'_i Y_{LM}(\theta'_i)Y_{00}(\theta'_i)\int b\ db\ J_M(qb) \times\{1-\exp[-\chi_0(b)-\chi_1(b)t(\Phi\prime)]\}. \tag{3.7}$$

On the other hand, if the target nucleus is spherically symmetric, but is susceptible to vibration around that spherical shape, R may be expressed as

$$R=R_0\left(1+\sum_{\lambda\mu}\alpha_{\lambda\mu}Y_{\lambda\mu}(\theta,\varphi)\right), \tag{3.8}$$

assuming that the target interaction to which an incident particle is subjected is described by an optical potential $U_P^{\rm opt}(r)$. Then we can expand $U_P^{\rm opt}(r)$ in powers of $\Sigma_{\lambda\mu}\alpha_{\lambda\mu}Y_{\lambda\mu}$ to get [17]

$$U_P^{\rm opt}(r)\simeq U_0(r)-\sum_{\lambda\mu}R_0\frac{d}{dr}U_0(r)\alpha_{\lambda\mu}Y_{\lambda\mu}(\theta,\varphi). \tag{3.9}$$

Now we consider a nucleus with a set of octupole vibrations and the relation between α_μ and phonon operator can be written as

$$\alpha_\mu=\frac{\beta_3}{\sqrt{7}}[b_\mu+(-)^\mu b^*_{-\mu}], \tag{3.10}$$

We shall assume that the nuclear excitation is small enough compared with the energy of the incident particle that it can be ignored. In such cases, the operator for the scattering amplitude between the nucleus and antiproton may be represented as

$$\hat{F}_v(q)=\frac{ik}{2\pi}\int d^2b e^{iq\cdot b} \times\left\{\delta_{f_i}-\exp\left[i\chi_{00}(b)+i\sum_\mu\chi_{3\mu}(B_\mu+B^+_\mu)\right]\right\}, \tag{3.11}$$

where

$$B_\mu=b_\mu e^{i\mu\varphi},\quad B^+_\mu=b^+_{-\mu}e^{-i\mu\varphi}. \tag{3.12}$$

Here we have assumed $\chi^+_{3\mu}=\chi_{3\mu}$, and

$$\chi_{00}(b)=-\frac{i}{2k}\int_{-\infty}^{\infty}dz U_0(r), \tag{3.13}$$

$$\chi_{3\mu}(b)\equiv\frac{i\beta_3R_0}{2\sqrt{7}R}\int_{-\infty}^{\infty}dz\frac{d}{dr}U_0(r)P_{3\mu}(0), \tag{3.14}$$

$$P_{3\mu}(0)=\begin{cases}O & \text{if } (3-\mu)=2S+1\\ (-)^{s+\mu}\left[\dfrac{7(3-\mu)!}{4\pi(3+\mu)!}\right]^{1/2}\dfrac{(2s+2\mu)!}{2^3s!(s+\mu)!} & \text{if } (3-\mu)=2s\end{cases} \tag{3.15}$$

with β_3 the octupole deformation parameters. Using the formulas of Baker, Campbell, and Hausdorff, we obtain the scattering amplitude between the zero-phonon ground state and the one-phonon excited state [16]

$$F_{LM}(q)=k\int_0^\infty b\ db\ J_M(qb)\chi_{LM}(b)e^{i\chi_N(b)}, \tag{3.16}$$

where

$$\chi_N(b)=\chi_{00}(b)+\chi_{cp}(b), \tag{3.17}$$

$$\chi_{cp}(b)=\frac{1}{2}\,i\sum_{LM}\chi^2_{LM}(b), \tag{3.18}$$

and for elastic scattering,

$$F_{00}(b)=ik\int_0^\infty b\ bd\ J_0(qb)[1-e^{i\chi_N}]. \tag{3.19}$$

The first term in Eq. (3.17) depends only on the ground state density of the target. The second term $\chi_{cp}(b)$ describes the effect of coupling the elastic with the (one-phonon) inelastic channels on the elastic phase in which the target nucleus makes a virtual transition to an excited state and then decays back to the ground state.

Now, we begin with the incident energy 179.7 MeV, where there exist $\bar{p}$-nuclei interaction experimental data. We take the values V_0 and W_0 calculated from formulas (3.7) and (3.19), and then adjust r_w, a_w, r_v, and a_v to fit the experimental data. The solid curves in Figs. 2–7 are our theoretical results. The experimental data are also given. We find that the optical potential given above can describe all of the experimental data. Hence from these results we are convinced that the optical potential determined by the above considerations can be used to predict the elastic and inelastic scattering differential cross sections at higher energies.

All of the optical potential parameters are considered as the following. W_0 is chosen as 135 MeV. V_0 is dependent on ϵ and decreases as the incident energy is higher than 1 GeV. Since W_0 is almost constant, r_w and a_w are the same values as at 179.7 MeV. We list all of the optical potential parameters at higher energies and the deformation parameters in Table II.

All calculated differential cross sections are given in Figs. 2–7. The antiproton energies 294.8 and 508 MeV, which are

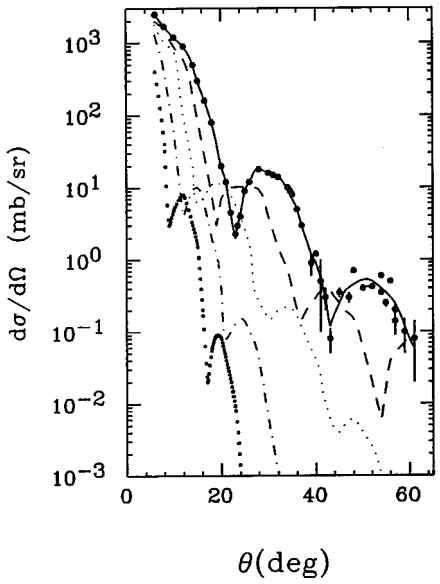

FIG. 2. Differential cross section for $\bar{p}$ elastic scattering on ^{12}C. —– 179.7 MeV, - - - - 294.8 MeV, ….. 508 MeV, –.–.–. 1070 MeV, and … … … 1833 MeV.

the existing LEAR beam energies [18], correspond to momenta 800 and 1100 MeV/c, respectively. Because the maximum energy of LEAR can reach the GeV region, we also calculated the differential cross section at 1.07 and 1.83 GeV. Our prediction shows that as the incident energy increases the diffraction patterns are more condensed. As the detection techniques are improved these patterns will be observed, at least in the region before the second or third minimum. We have assumed the $\bar{p}$-neutron and $\bar{p}$-proton interactions are the same. At the higher energies considered in this paper, one may expect the Coulomb interaction to be small and we omit it from the calculations.

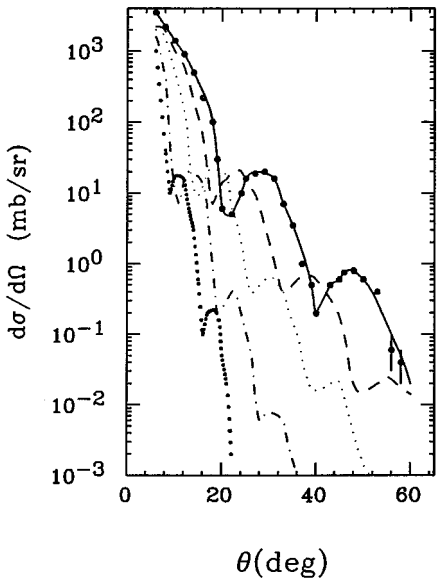

FIG. 3. Differential cross section for $\bar{p}$ elastic scattering on ^{16}O. —— 178.4 MeV. The other curves have the same meaning as in Fig. 2.

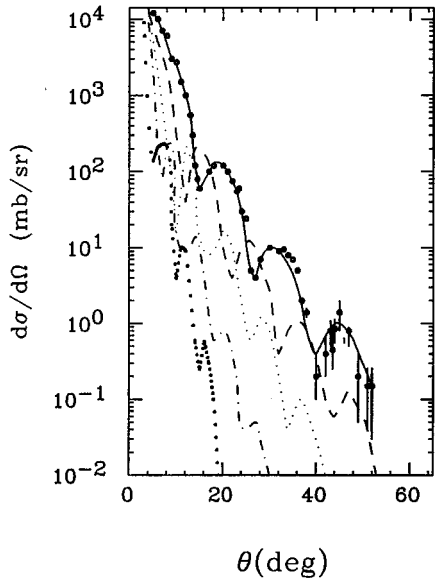

FIG. 4. Differential cross section for $\bar{p}$ elastic scattering on ^{40}Ca. The curves have the same meaning as in Fig. 3.

Antiproton inelastic scattering to the ^{12}C 4.43 MeV 2^+ state is treated in the framework of the usual rotational model. As suggested from the analysis of proton inelastic scattering [21] only a quadrupole deformation was taken into account and no hexadecapole deformation was included. The best fits so obtained are displayed as the solid curve in Fig. 6. The experimental data are from Ref. [5]. Simultaneously the theoretical results at higher energies are predicted.

To describe the 3^- (9.6 MeV) level, a calculation has been done in the framework of the octupole vibrational model. The results are displayed as the solid curve in Fig. 7 for the 179.7 MeV data; this corresponds to the parameters given in Table II. The angular distribution of the 3^- state is

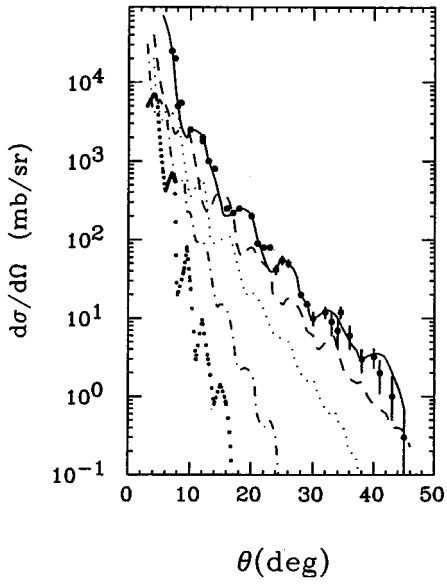

FIG. 5. Differential cross section for $\bar{p}$ elastic scattering on ^{208}Pb. —– 180.3 MeV. The other curves have the same meaning as in Fig. 2.

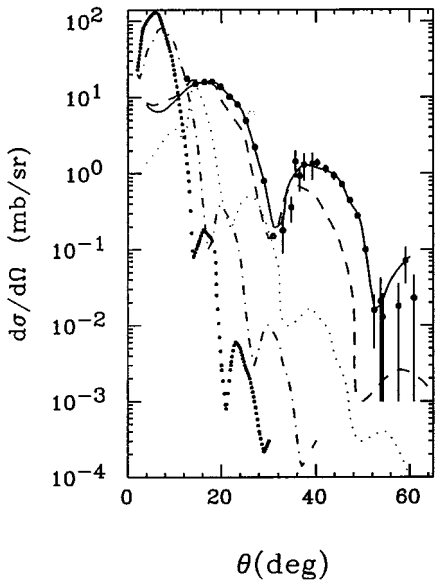

FIG. 6. Differential cross section of inelastic scattering of antiproton to the 4.4 MeV, 2^+ excited state measured at 179.7 MeV incident energy. —– 179.7 MeV, - - - - 294.8 MeV, ….. 508 MeV, –.–.–. 1070 MeV, and … … … 1833 MeV.

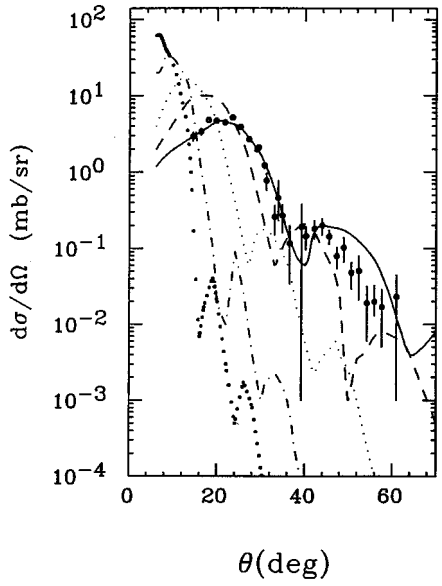

FIG. 7. Differential cross section of inelastic scattering of antiproton to the 9.6 MeV, 3^- excited state measured at 179.7 MeV incident energy. —- 294.6 MeV. The other curves have the same meaning as in Fig. 6.

not very well described at backward angles where it clearly exhibits too much diffraction. Simultaneously the theoretical results at 294.6, 508, 1070, and 1833 MeV energies are predicted.

IV. CONCLUSION

Let us enumerate the main results of this investigation.

(1) The antiproton optical potential is derived from multiple scattering theory and the impulse approximation. The

TABLE II. Optical potential parameters and deformation parameters for $\overline{p}$-nucleus elastic and inelastic scattering.

Nucleon	$E_{\overline{P}}$ (MeV)	W_0 (MeV)	V_0 (MeV)	r_w (fm)	r_v (fm)	a_w (fm)	a_v (fm)	β_2 [19]	β_3 [20]
	179.7	135	35	1.05	1.2	0.54	0.54		0.33
	294.8	135	35	1.05	1.2	0.54	0.54		0.40
^{12}C	508	135	35	1.05	1.2	0.54	0.54	0.592	0.36
	1070	135	20	1.05	1.3	0.54	0.54		
	1833	135	10	1.05	1.4	0.54	0.54		
	178.4	135	35	1.05	1.2	0.54	0.54		
	294.8	135	35	1.05	1.2	0.54	0.54		
^{16}O	508	135	35	1.05	1.2	0.54	0.54		
	1070	135	20	1.05	1.3	0.54	0.54		
	1833	135	10	1.05	1.4	0.54	0.54		
	179.8	135	35	1.15	1.25	0.6	0.55		
	294.8	135	35	1.15	1.25	0.6	0.55		
^{40}Ca	508	135	35	1.15	1.25	0.6	0.55		
	1070	135	20	1.15	1.4	0.6	0.55		
	1833	135	10	1.15	1.45	0.6	0.55		
	180.3	135	35	1.15	1.3	0.7	0.6		
	294.8	135	35	1.15	1.3	0.7	0.6		
^{208}Pb	508	135	35	1.15	1.3	0.7	0.6		
	1070	135	20	1.15	1.4	0.7	0.6		
	11 833	135	10	1.15	1.5	0.7	0.6		

optical potential strengths are determined by $\overline{pN}$ scattering experimental data. It is found that the imaginary part strengths W_0 of the optical potential are nearly constant at incident energies from 180 to 1833 MeV. The imaginary part strengths W_0 of the optical potential are at least fourfold times larger than the real part strength V_0 and decrease with increasing energies. Therefore the antiproton optical potential is a strong absorption.

(2) The magnitude and sign of the real part V_0 and the imaginary part W_0 are determined by the behavior of ϵ and $\sigma_{\overline{pN}}$ for the $\overline{pN}$ elementary amplitude, and these two parameters have been determined from the experimental data. Therefore the antiproton optical potentials obtained are quite dependable.

(3) At low energies (e.g., 179.7 MeV), the optical potential obtained can fit all of the $\overline{p}$-A elastic and inelastic scattering data. The clear diffraction patterns, the absolute values, and positions of the differential cross section at the peaks and dips of the angular distributions can be seen from the figures. Because the theoretical results fit very well the experimental data at 179.7 MeV, we believe that the theoretical curves at higher energies are close to the experimental tendency.

We would like to thank X. Y. Shen and Y. B. Dong for their assistance with the computational program.

[1] D. Garreta *et al.*, Phys. Lett. **135B**, 266 (1984); Phys. Lett. **139B**, 464 (1984).
[2] D. Garreta *et al.*, Phys. Lett. **149B**, 64 (1984); Phys. Lett. **151B**, 473 (1985).
[3] V. Ashford *et al.*, Phys. Rev. C **30**, 1080 (1984).
[4] W. Brückner *et al.*, Phys. Lett. **158B**, 180 (1985).
[5] M.-C. Lemaire *et al.*, Nucl. Phys. **A456**, 557 (1986).
[6] S. Janouin *et al.*, Nucl. Phys. **A451**, 541 (1986); O. D. Dalkarov and V. A. Karmanov, Nucl. Phys. **A445**, 579 (1985).
[7] C. Y. Wong *et al.*, Phys. Rev. C **29**, 441 (1984).
[8] Li Yang-guo, High Energy Phys. Nucl. Phys. **17**, 199 (1993); **18**, 186 (1994).
[9] A. K. Kerman *et al.*, Ann. Phys. (N.Y.) **8**, 551 (1959).
[10] H. Kaseno *et al.*, Phys. Lett. **61B**, 102 (1976); **68B**, 487 (1977).
[11] P. Jenni *et al.*, Phys. Lett. **94B**, 1 (1975).
[12] Li Yangguo, High Energy Phys. Nucl. Phys. **12**, 501 (1988); Zhang Yu-shun, Chin. J. Nucl. Phys. **12**, 309 (1990).
[13] R. Klapisch, Nucl. Phys. **A434**, 207 (1985).
[14] P. Jenni *et al.*, Nucl. Phys. **B94**, 1 (1975).
[15] H. Kaseno *et al.*, Phys. Lett. **61B**, 203 (1976); **68B**, 487 (1977).
[16] Zhang Yu-shun, J. Math. Phys. **30**, 1368 (1989).
[17] T. Tamura, Rev. Mod. Phys. **37**, 679 (1965).
[18] A. Martin *et al.*, Nucl. Phys. **A487**, 567 (1988).
[19] S. Raman *et al.*, At. Data Nucl. Data Tables **36**, 1 (1987).
[20] R. H. Spear, At. Data Nucl. Data Tables **42**, 55 (1989).
[21] R. De Leo *et al.*, Phys. Rev. C **28**, 1443 (1983).